Int. J. Electrochem. Sci., 14 **(2019)** 11616 – 11629, doi: 10.20964/2019.12.67

International Journal of
ELECTROCHEMICAL
SCIENCE
www.electrochemsci.org

Synthesis and Electrochemical Properties of Na and Mg co-Doped $LiFe_{0.65}Mn_{0.35}PO_4$ /C Cathode Materials for Lithium-Ion Batteries

Shunpan Qiao[1], Lingzhi Zhu[2], Enshan Han[3,], Lina Li[4], Chenyu Du[5], Yanzhen He[6,*]*

[1] School of Chemical Engineering and Technology, Hebei Universityof Technology, Tianjin 300130, PR China,email address:2269366910@qq.com
[2] Tianjin.CN email address:lzhu@hebut.edu.cn
[3] Tianjin.CN
[4] School of Chemical Engineering and Technology, Hebei Universityof Technology, Tianjin 300130, PR China,email address:1206929370@qq.com
[5] School of Chemical Engineering and Technology, Hebei Universityof Technology, Tianjin 300130, PR China,email address:491479520@qq.com
[6] School of Chemical Engineering and Technology, Hebei Universityof Technology, Tianjin 300130, PR China
[*]E-mail: eshan@hebut.edu.cn, yzhe87@163.com

Received: 8 July 2019 / *Accepted:* 25 August 2019 / *Published:* 29 October 2019

In this paper, $Li(Fe_{0.65}Mn_{0.35})_{0.98}Mg_{0.02}PO_4/C$, $Li_{0.98}Na_{0.02}Fe_{0.65}Mn_{0.35}PO_4/C$ and $Li_{0.98}Na_{0.02}(Fe_{0.65}Mn_{0.35})_{1-x}Mg_xPO_4/C$ (x = 0.01, 0.02, 0.03, 0.05) were successfuly synthesized by sol-gel method and modified by Na^+ doped and Mg^{2+} doped. The effects of Na^+ and Mg^{2+} doping on the structure, morphology and electrochemical performance of $LiFe_{0.65}Mn_{0.35}PO_4/C$ were investigated by X-ray diffraction (XRD), scanning electron microscopy (SEM), Energy Dispersive Spectroscopy (EDS), and electrochemical tests. The results show that when x=0.03, the material has the best electrochemical performance. The first discharge capacity at 0.1 C is as high as 147.7 $mAhg^{-1}$ (1 C=170.2 $mAhg^{-1}$) at the potential range of 2.5–4.5 V, When returning to 0.1 C after 40 cycles, the discharge specific capacity is still up to 142.1 $mAhg^{-1}$. In addition, the Rct values and the Li^+ diffusion coefficient of Na0.02Mg0.03 were 215.2 Ω, 4.501×10^{-14} cm^2s^{-1}, respectively.

Keywords: Lithium-ion battery, sol-gel method, $LiFe_{0.65}Mn_{0.35}PO_4/C$, Na^+doping, Mg^{2+}doping

1. INTRODUCTION

In the past two decades, Padhi and Goodenough et al. found that $LiMPO_4$ (M=Mn, Fe, Co, Ni) had an ordered olivine structure [1]. Due to its non-toxicity, low cost, good electrochemical performance and high thermal stability, it is widely recognized in cathode materials [2-3].

After many studies in recent years, the $LiFePO_4$ material is relatively mature [4-5]. Its reversible capacity is close to the theoretical value, but the low working voltage (3.4 V vs. Li^+/Li) leads to a low energy density (586 $Whkg^{-1}$=170 $mAhg^{-1}$×3.45V). Compared with that of $LiFePO_4$, $LiMnPO_4$ has a higher working potential (4.1 V vs. Li^+/Li) and theoretical energy density (701 $Whkg^{-1}$=171$mAhg^{-1}$×4.1 V) [6]. In general, the working voltage of the $LiMnPO_4$ material is within the stable electrochemical window [7] of the currently used electrolyte; additionally, the $LiMnPO_4$ is considered to balance the lattice distortion caused by the Jahn-Teller effect of $LiMnPO_4$ and the dissolution of manganese between electrolytes [8]. Considering the solid solution structure of $LiFe_xMn_{1-x}PO_4$ material [9-18], some researchers have attempted to improve its electrochemical performance. In terms of material composition, the introduction of Mn is equivalent to utilizing the high voltage of $LiMnPO_4$, while the Fe is consider to be utilizing the high conductivity of $LiFePO_4$. Therefore, increasing the mixed transition metal phosphate is a powerful method to improve the electrochemical properties [19]. Due to the larger radius of Mn^{2+}, doping Mn^{2+} in the crystal lattice can broaden the lithium ion diffusion channel, while the presence of Fe^{2+} can improve the electrode kinetics and this combination makes the material exhibit excellent electrochemical performance [20]. The structure of $LiFe_xMn_{1-x}PO_4$ is olivine which is similar to $LiFePO_4$ (or $LiMnPO_4$). Thus, $LiFe_xMn_{1-x}PO_4$ belongs to the orthorhombic system, and the space group is Pnmb, The cell parameters are between $LiFePO_4$ and $LiMnPO_4$.

To improve the electrochemical performance of $LiFePO_4$, $LiMnPO_4$ and composite materials, numerous studies have established that multi-element doping can lead to better electrochemical performance than single doping. As with Shu and others, Ni/Mn co-doped $LiFePO_4$ composites were synthesized by the solid state method [21]. Co-doping can effectively improve the electrochemical performance, for instance, $LiFe_{0.95}Ni_{0.02}Mn_{0.03}PO_4/C$ has excellent rate and cycle performance. Wang et al. successfully synthesized Na^+, Cl^- co-doped $LiFePO_4$ materials with improved capacity, columbic efficiency and rate performance [22]. This can be attributed to the lattice distortion and electronic conductivity. Using the Na/Ti co-doping method [23], Shu et al. successfully present the $Li_{1-x}Na_xFe_{1-x}Ti_xPO_4/C$ composites. The $5LiMn_{0.9}Fe_{0.1}PO_4 \cdot Li_3V_2(PO_4)_3/C$ composite cathode that was synthesized by Wu [24], which also exhibited a high reversible capacity of 158.1 mAh/g at 0.05C. Additionally, there are Zr^{4+}-Co^{2+} co-doping materials [25-26] as well as others. Thus, the co-doping is a powerful method to improve the properties of $LiMnPO_4$. Currently, the systems of Fe^{2+}-Mg^{2+} [27-35], Co^{2+}-Mg^{2+} [36], Fe^{2+}-Co^{2+} [37-38], Fe^{2+}-Zn^{2+} [39], Fe^{2+}-Ti^{4+} [40], and Fe^{2+}-Nb^{5+} [41], have achieved co-doping, and they all improve the electrochemical properties. For example, the discharge capacity of $Li_{0.995}Nb_{0.005}Mn_{0.85}Fe_{0.15}PO_4/C$ at 0.2 C and 0.5 C is 166 and 153 $mAhg^{-1}$, respectively. while the discharge capacities of $LiMnPO_4/C$ are only 138 and 107 $mAhg^{-1}$, respectively .Therefore, the electrochemistry capability of $LiMnPO_4/C$ is significantly enhanced by Fe^{2+}-Nb^{5+} co-doping [41]. In short, a material with various elements co-doped will obtain better electrochemical performance than single doping.

In the previous reports, Na^+ and Mg^{2+} doping in the materials of $LiFePO_4$ and $LiMnPO_4$ can significantly improve the rate and cycle performance of phosphate-based cathode materials. However, few researchers have addressed the problem of co-doping of Na^+ and Mg^{2+} in $LiFe_{1-x}Mn_xPO_4$ composites. Therefore, we will proceed to $Li_{0.98}Na_{0.02}(Fe_{0.65}Mn_{0.35})_{1-x}Mg_xPO_4$ after $LiFe_{0.65}Mn_{0.35}PO_4/C$ is separately doped with Na^+ and Mg^{2+} to select the best doping ratio. and successfully synthesize Mg-

doped $Li_{0.98}Na_{0.02}(Fe_{0.65}Mn_{0.35})_{1-x}Mg_xPO_4$ (x=0.01, 0.02, 0.03, 0.05) at the Fe and Mn sites of the lithium ion battery cathode materials. A sol-gel method was utilized, and the structure, morphology and electrochemical properties of these materials studied in detail.

2. EXPERIMENTAL

2.1 Synthesis

The composite of $Li(Fe_{0.65}Mn_{0.35})_{0.98}Mg_{0.02}PO_4/C$ (Mg0.02) , $Li_{0.98}Na_{0.02}Fe_{0.65}Mn_{0.35}PO_4/C$ (Na0.02), and $Li_{0.98}Na_{0.02}(Fe_{0.65}Mn_{0.35})_{1-x}Mg_xPO_4/C$ (Na0.02Mgx) (x=0.01, 0.02, 0.03, 0.05) were synthesized by a sol-gel method. Stoichiometric amounts of a Mn source ($Mn(CH_3COO)_2\cdot4H_2O$), C source (citric acid) (C to product molar mass ratio of 3:10), P source ($NH_4H_2PO_4$), Fe source ($FeCl_2\cdot4H_2O$) and Li source ($CH_3COOLi\cdot2H_2O$) were sequentially dissolved in 150 mL of deionized water, and corresponding amounts of a Na source ($CH_3COONa\cdot3H_2O$) and Mg source ($Mg(CH_3COO)_2\cdot4H_2O$) were added to the mixed solution in front. Then the obtained solution was heated and stirred in a 70 °C water bath until a pale green wet gel formed. The products were furtherdried at 80 °C in a vacuum oven and ground with an agate mortar. After this, the mixture was preheated in a tube furnace at 350 °C for 5 h in a N_2 protective atmosphere tube furnace. After natural cooling, the obtained precursor was calcined under a N_2 atmosphere at 750 °C for 10 h (the heating rate of both calcinations was maintained at 5 $^oC\ min^{-1}$), after a final natural cooling stage, the Mg0.02, Na0.02 and Na0.02Mgx (x=0.01, 0.02 , 0.03, 0.05) were obtained . The carbon content in the material was 30%.

2.2 Preparation of positive film and battery assembly

The prepared positive electrode material was dissolved in N-methylpyrrolidone (NMP) with acetylene black and polyvinylidene fluoride (PVDF) at a mass ratio of 8:1:1 to obtain a uniformly dispersed slurry. It was coated on an aluminum foil and dried under vacuum at 110 °C for 10 h. At the end, the dried aluminium foil was compacted by a tableting machine and punched into a circular piece, The pieces had a diameter of approximately 10 mm and an average mass of 2.5 to 3 mg cm^{-2} of active material, which were used as the positive electrode.

A mixed solution of EC, EMC and DMC (volume ratio 1:1:1) containing 1 M $LiPF_6$ was used as the electrolyte. The CR2032 coin cell was assembled in an inert gas-protected glove box, and the battery was sealed and allowed to stand for 24 h.

2.3 Physical characterization and electrochemical testing

The crystal structures were measured by an X-ray diffraction (XRD) analyser (D8-Fouse, made in Germany), using Cu Ka radiation. The tube voltage and current were fixed at 40 kV, and 40 mA, respectively. and the step width was 0.02°. The scanning speed was 12°/min, and the test range was 2θ=10-80°. The morphology and microstructure of the powder were analysed by scanning electron

microscopy (SEM, Nova Nano SEM 450 FEI). The type and distribution of the surface elements of the sample in the powder can be obtained by EDS analysis of the material using an EDAX spectrometer (manufactured by AMETEK in the USA, Model OCTANE PLUS).

The material was subjected to constant current charge/discharge performance using a LAND CT-2001 battery test system with a voltage range of 2.5-4.5 V (vs. Li^+/Li). The cyclic voltammograms (CV) and electrochemical impedance spectroscopy (EIS) measurements were both carried on a CHI660C electrochemical workstation at room temperature.with a voltage range of 2.5-4.5 V (vs. Li^+/Li) and a scan rate of 0.1 mVs^{-1}. The frequency range was 10^5-0.01 Hz and the amplitude was 5 mV. EIS data were analysed using ZsimpWin 3.10 software.

3. RESULTS AND DISCUSSION

3.1. Structure and morphology

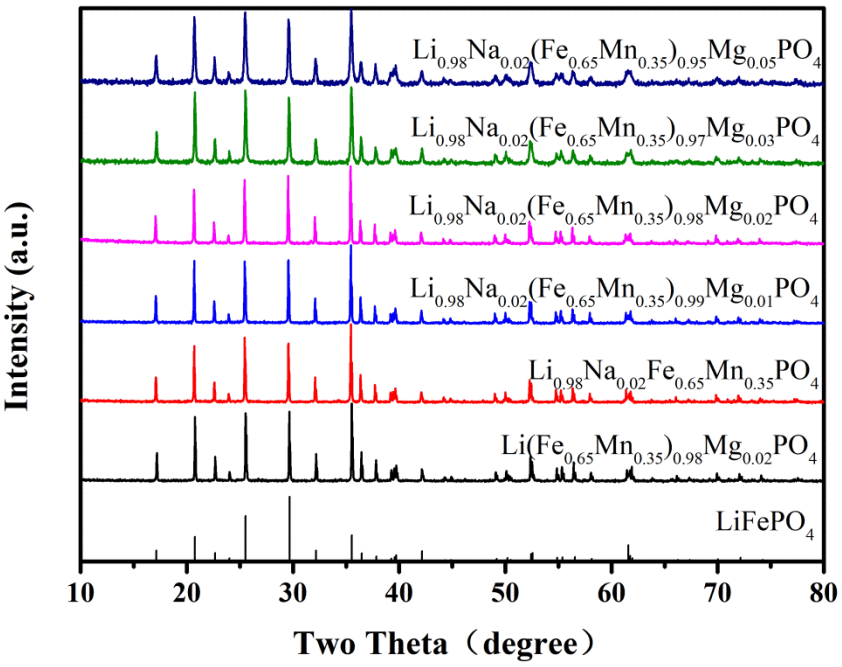

Figure 1. XRD patterns of Mg0.02、Na0.02、Na0.02Mgx (x=0.01,0.02,0.03,0.05)

The patterns of $Li(Fe_{0.65}Mn_{0.35})_{0.98}Mg_{0.02}PO_4/C$, $Li_{0.98}Na_{0.02}Fe_{0.65}Mn_{0.35}PO_4/C$ and $Li_{0.98}Na_{0.02}(Fe_{0.65}Mn_{0.35})_{1-x}Mg_xPO_4/C$ (x=0.01,0.02,0.03,0.05) are shown in Figure 1. It is clear that all samples are purely ordered olivine compounds with an orthorhombic structure (space group Pnma) [42]. The results clearly show that Na^+ and Mg^{2+} doping does not destroy the main structure of the $LiFe_{0.65}Mn_{0.35}PO_4/C$. In other words, the co-doping of Na^+ and Mg^{2+} in the combined system also keeps the orthorhombic structure. All materials have the characteristic peaks of $LiFePO_4$ (JCPDS No. 40−1499). However, as the amount of doping changes, the sharpness of the diffraction peak slightly changes and no impurity peak is found. As show in Figure 1, the doped Na and Mg in the

$LiFe_{0.65}Mn_{0.35}PO_4/C$ composite was successfully formed olivine structures with high crystallinity. Except for this, no diffraction peaks for crystalline carbon were detected, which may have contributed to the amorphous residual carbon in the composite.

Table 1. Lattice parameters of Mg0.02、Na0.02、Na0.02Mgx(x=0.01,0.02,0.03,0.05)

Samples	a/(Å)	b/(Å)	c/(Å)	V(Å^3)	Rwp(%)
Mg0.02	10.3708734	6.0404158	4.7124728	295.20997	11.53
Na0.02	10.3786524	6.0434601	4.7129822	295.61225	11.9
Na0.02Mg0.01	10.3755158	6.0411047	4.7108469	295.27389	11.44
Na0.02Mg0.02	10.3708610	6.0404249	4.7124750	295.21021	11.6
Na0.02Mg0.03	10.3717708	6.0391590	4.7109941	295.08146	11.64
Na0.02Mg0.05	10.3684719	6.0380196	4.7114877	294.96286	12.17

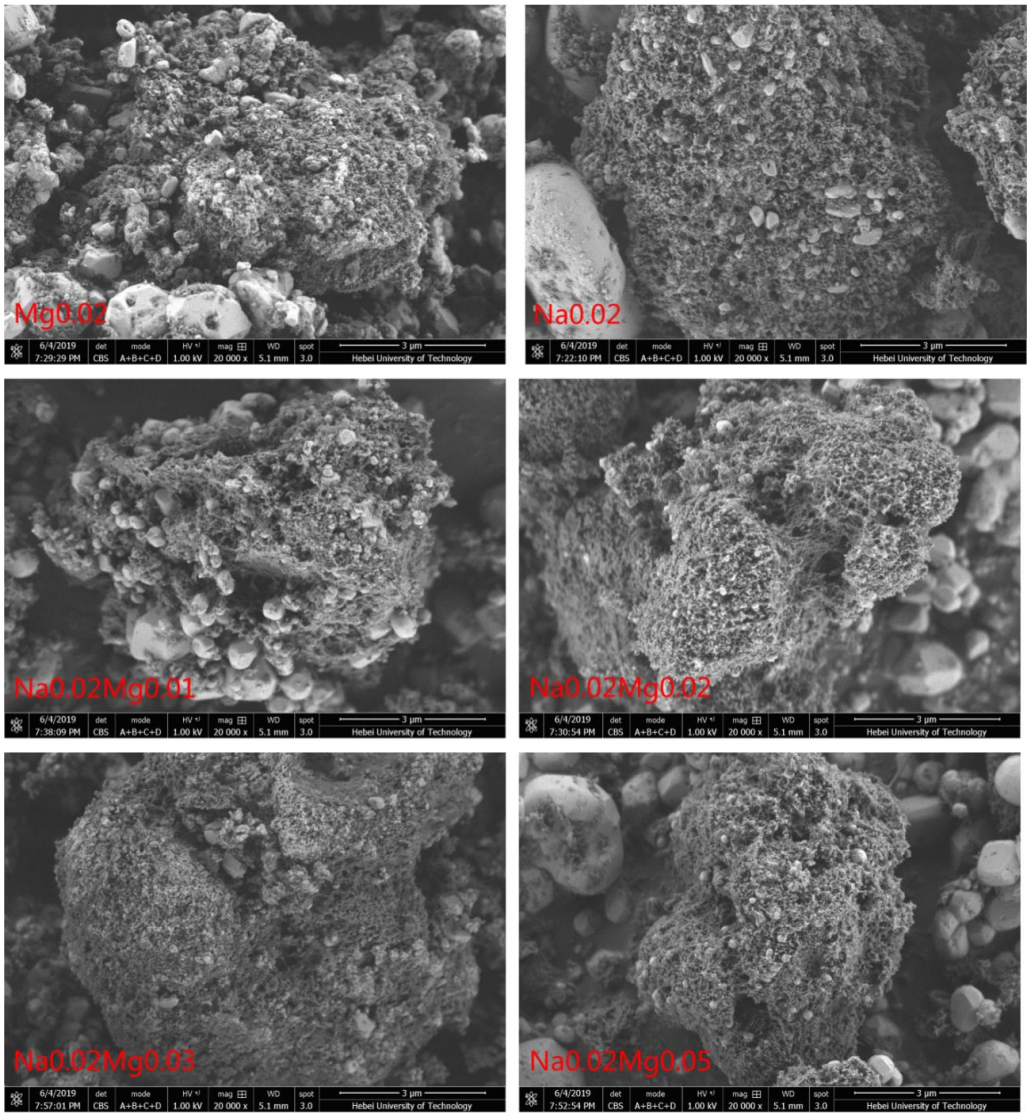

Figure 2. SEM images of Mg0.02、Na0.02、Na0.02Mgx (x=0.01,0.02,0.03,0.05)

Table 1 displays the lattice parameters of the co-doped system. The cell coefficients of the six doped lithium iron manganese phosphates are larger than those of lithium iron phosphate ($LiFePO_4$) [43], and the increase of the unit cell volume can provide a larger ionic radius space for migration, and accelerate the diffusion of lithium ions [44]. Table 1 shows that, when the Na^+ doping amount is 0.02, because of the Mg^{2+} ion radius is smaller than the ionic radius of Fe^{2+} and Mn^{2+}, the unit cell volume decreases slightly with the increasing doping amount. And the regularly are visible in the Table 1 of Rwp. All the values of the Rwp are less than 15%. and within the reasonable range allowed, Thus,we can conclude that the sample has certain accuracy in the cell refinement process.

The SEM image of the prepared sample is shown in Figure 2. All of the samples have a distinctt pore-like structure with some blocky structure. There are many pore gaps on the surface of the sample. As shown, when the doping of Na^+ is 0.02, and the doping amount of Mg^{2+} is 0.03, the particles have obvious pores, and the specific surface area is large, making the structure more permeable and providing the electrolyte easy to contact with the materials. there are few other similar block structures. Other samples also have obvious pores, which facilitate ion flow. However, if there is a relatively obvious block structure, and carbon is completely coated on the surface, it is not conducive to ion flow.

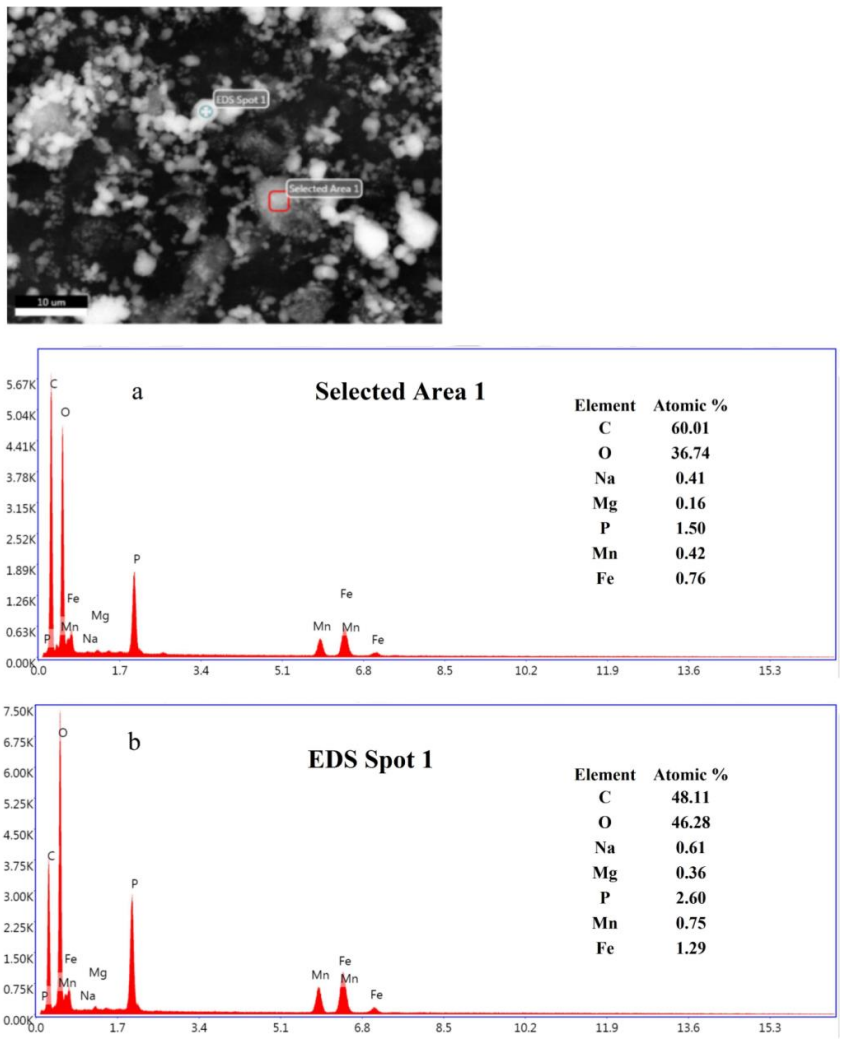

Figure 3. a-b EDS images of $Li_{0.98}Na_{0.02}(Fe_{0.65}Mn_{0.35})_{0.97}Mg_{0.03}PO_4/C$

The EDS spectrum at x=0.03 is shown in Figure 3a-b, excluding the undetected Li element, because X-ray fluorescence is extremely low for elements such as Li or Be [45]. All elements are present in the composite. It should be noted that the relative content of the elements in these two regions are the same. The pore structure is chosen and the particles are filled with pores at zone 1. For Region 2, the block-like structure is chosen. It can be seen from the ratio of C to O, that region 1 consists of a higher carbon content.

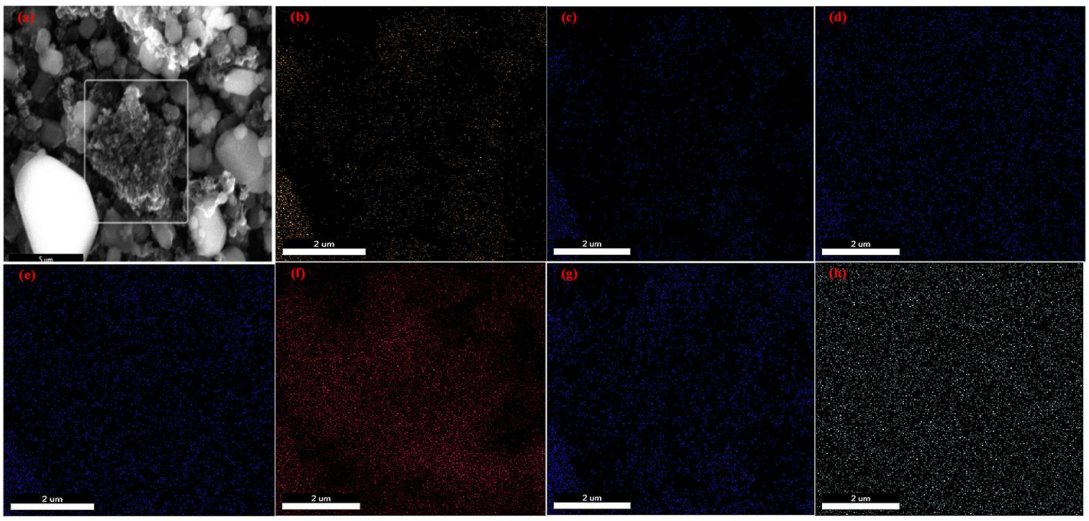

Figure 4. (Colour online) Elemental mapping of Na0.02Mg0.03. a, SEM; b, Na mapping; c, Mg mapping; d, Mn mapping; e, Fe mapping; f, O mapping; g, P mapping; h, C mapping.

The carbon was distributed in an amorphous state between the particles or on the surface of the particles to form a pore structure. In addition, carbon can not only act a be used as a conductive and reducing agent, but also prevent particle agglomeration. which can shorten the diffusion path of lithium ions and provide a good electron transport channel for its deintercalation. This can be observed from the ratio of Fe to Mn in that no matter which structure is chosen, it is close to the theoretical value.

Figure 4 shows the distribution of the elements in Na0.02Mg0.03. The elements in the sample are relatively homogenous distribution. From the EDS mappings, the elements of Na, Mg, Mn, and Fe are distributed in each nanoparticle of Na0.02Mg0.03.

3.2. Electrochemical performance

Figure 5 presents the potential curves for the prepared samples with a voltage range of 2.5 - 4.5 V vs Li^+/Li and a scan rate of 0.1 mVs^{-1}. Two pairs of redox peaks are $Mn^{2+}/Mn^{3+}$and Fe^{2+}/Fe^{3+}, respectively. Comparing the CV curves, all samples have a similar trend, but the redox peak current value of x=0.03 in the doping material is higher and clearer than that of the other x values. We can conclude that the sample Na0.02Mg0.03 has excellent electrochemical performance.

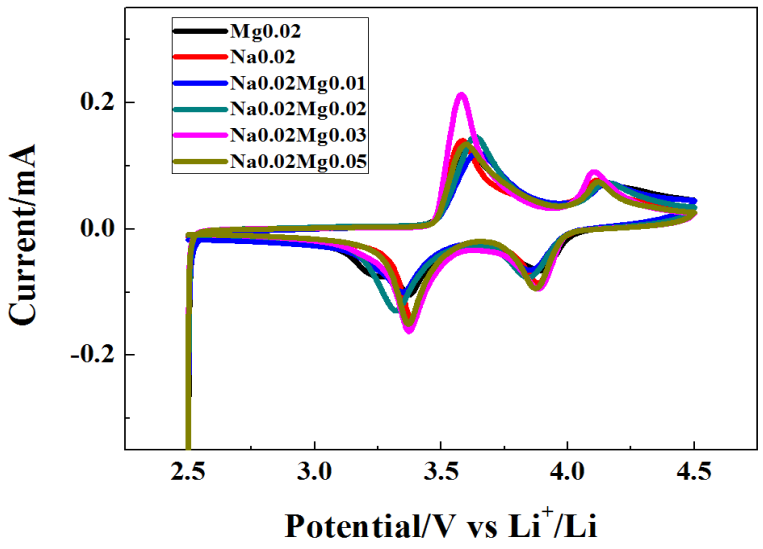

Figure 5. CV curves of Mg0.02、Na0.02 and Na0.02Mgx(x=0.01,0.02,0.03,0.05)

The first charge/discharge curve of the prepared sample at 0.1 C is shown in the Figure 6. As indicated in Figure 6, there are two pairs of redox peaks at approximately 4.1 V/3.9 V and 3.5 V/3.4 V, corresponding to the redox reaction of Mn^{3+}/Mn^{2+} and Fe^{3+}/Fe^{2+}, respectively. The initial discharge capacities of Mg0.02, Na0.02, Na0.02Mg0.01, Na0.02Mg0.02, Na0.02Mg0.03 and Na0.02Mg0.05 were 139, 136.3, 130.3, 144.2, 147.7 and 141 $mAhg^{-1}$, respectively. The coulombic efficiencies were 82.89%, 83.93%, 86.12%, 87.93%, 88.92%, and 87.80%, respectively. The Na0.02Mg0.03 has the largest efficiencies, which means that it is the best ratio for improving the electrochemical properties.

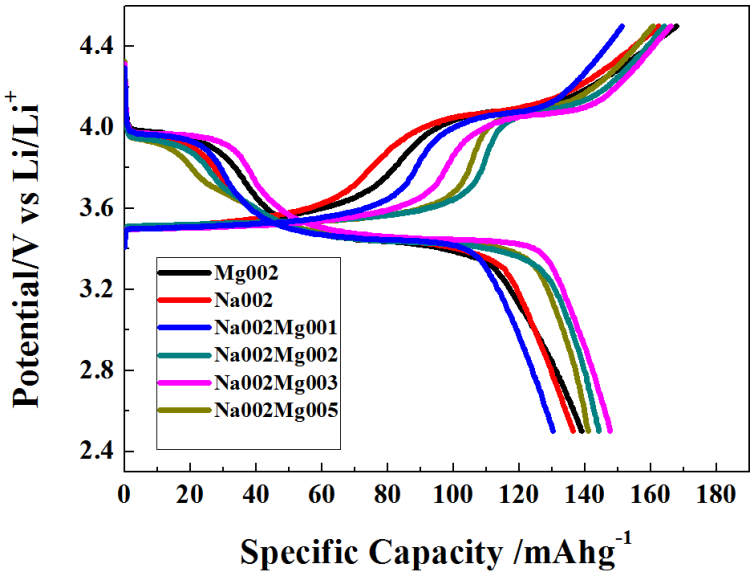

Figure 6. Initial charge-discharge curves of Mg0.02、Na0.02 and Na0.02Mgx (x=0.01,0.02,0.03,0.05) under 0.1 C

The above results indicate that an appropriate amount of Na^+ and Mg^{2+} doping can effectively increase the charge/discharge capacity of the material. The doping of Na and Mg may also contribute to

an increase in the diffusion capacity of Li^+. In addition, the doping material discharge capacity is less than the charge capacity, which demonstrates that the Li^+ interval and separation are incomplete during charging. Compared with that of the other samples, the sample Na0.02Mg0.03 has a stable voltage platform. All in all, the Na0.02Mg0.03 is the best choice for the electrode materials. The high discharge capacity and cycle stability are consistent with the porous structure shown by the previous SEM with gaps, which greatly promotes electrolyte penetration and promotes lithium ion diffusion and electron transport.

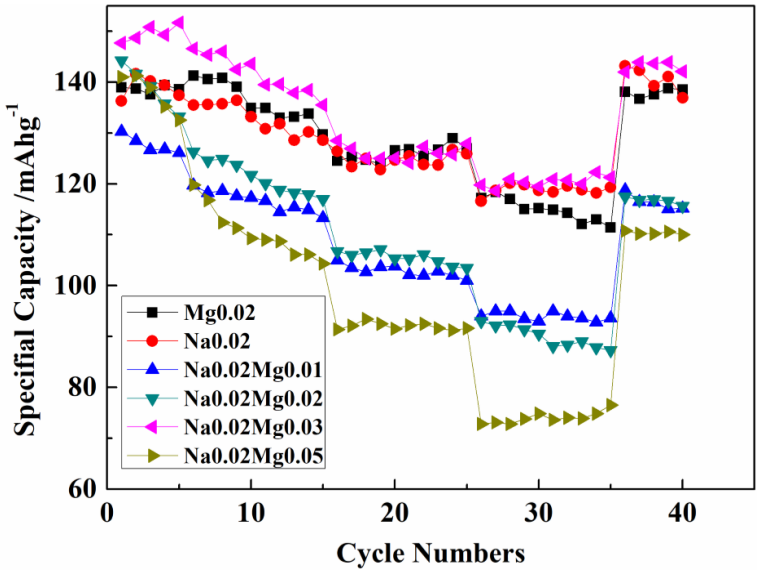

Figure 7. Cyclic performance at different rates of Mg0.02、Na0.02 and Na0.02Mgx(x=0.01,0.02,0.03,0.05)

The cyclic performance is a parameter to evaluate the stability of electrode materials. To further study the battery performance, we conduct the cycle performance of the prepared samples is measured at different rates of 0.1 C, 0.2 C, 0.5 C and 1.0 C. Figure 7 shows the curves of cyclic performance. The proper amount of Na^+ and Mg^{2+} doping can improve the rate performance of the material and enhance the structural stability the material. After multiple charge and discharge cycles and a final return to 0.1 C, the capacity retention rates of Mg0.02, Na0.02, Na0.02Mg0.01, Na0.02Mg0.02, Na0.02Mg0.03 and Na0.02Mg0.05 were 99.40%, 100.44%, 88.41%, 80.17%, 96.21% and 78.01%, respectively. The Mg0.02, Na0.02 and Na0.02Mg0.03 exhibits a discharge specific capacity that is relatively more stable and a higher capacity retention. The sample Na0.02Mg0.03 in particular has a first discharge capacity as high as 147.7 $mAhg^{-1}$ at 0.1 C , and after returning to 0.1 C, the discharge specific capacity is still up to 142.1 $mAhg^{-1}$. It can be concluded that Na and Mg doping can increase the initial discharge capacity and cycle stability performance of the $LiFe_{0.65}Mn_{0.35}PO_4/C$ cathode. From Table 2, we can see that the synthesized sample has a higher discharge specific capacity at 0.1 C by comparison to that of the others. Additionally Simultaneously, Figure 7 also shows that the rate performance of the sample needs further research to improve.

Table 2. Electrochemical performance of the ion co-doped material described in the literature.

Compound	Method	Best X value	C-Rate	Capacity($mAhg^{-1}$)	Reference
$LiFe_{1-x-y}Ni_xMn_yPO_4/C$ (x=0.01-0.04;y=0.04-0.01)	solid-state reaction	0.02	0.1 C	145.4	[21]
$Li_{0.99}Zr_{0.0025}Fe_{1-x}Co_xPO_4$ (x=0.005,0.001,0.015,0.02)	solid-state reaction	0.001	0.1 C	139.9	[25]
$Li_{1-x}Zr_{x/4}Fe_{0.99}Co_{0.01}PO_4$ (x=0.005, 0.01, 0.015, 0.02)	solid-state reaction	0.01	0.1 C	130.0	[26]
$LiMn_{0.8}Fe_{0.19}Mg_{0.01}PO_4/C$	solid-state reaction		0.1 C	145.0	[33]
$LiMn_{0.9}Fe_{0.1-x}Mg_xPO_4/C$ (x = 0, 0.01, 0.02, 0.05)	solid-state reaction	0.01	0.1 C	143.0	[34]
$LiMn_{0.9}Fe_{0.05}Mg_{0.05}PO_4$	solid-state reaction		0.1 C	140.0	[35]
$LiMn_{0.9}Fe_{0.1-x}Co_xPO_4/C$ (x = 0, 0.05 and 0.1)	solid-state reaction	0.05	0.05 C	145.0	[38]
$LiMn_{0.9}(FeZn)_{0.05}PO_4/C$	solid-state reaction		0.1 C	151.3	[39]
$Li(Mn_{0.85}Fe_{0.15})_{0.92}Ti_{0.08}PO_4/C$	solid-state reaction		0.2 C	154.0	[40]
$Li_{0.98}Na_{0.02}(Fe_{0.65}Mn_{0.35})_{1-x}Mg_xPO_4/C$ (x = 0.01, 0.02, 0.03, 0.05)	sol-gel method	0.03	0.1C	147.7	This work

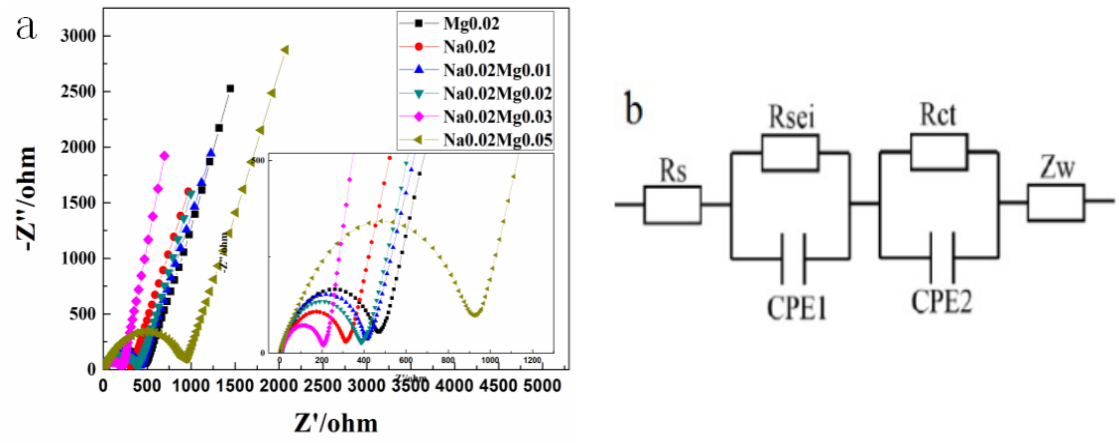

Figure 8. a–b Electrochemical impedance (EIS) spectra of Mg0.02、Na0.02 and Na0.02Mgx (x=0.01,0.02,0.03,0.05) samples and equivalent circuit diagram

The alternating current impedance spectrumand of the prepared sample showing the impedance of the doped material of Na^+ and Mg^{2+} is displayed in the Figure 8a. The EIS results of the prepared samples were calculated with ZSimpWin software, and Figure 8b describes the equivalent circuit

diagram corresponding to the ZSimpWin impedance simulation analysis. Each Nyquist plot consists of three parts: the high-frequency area abscissa intercept point, the mid-frequency area semi-circle area, and the inclined straight line in the low-frequency area The fitting results of the data for the electrochemical impedance curves are shown in Table 3. The electrolyte resistance, electrode interface resistance, and charge transfer resistance are represented by Rs, Rsei, and Rct, respectively. TheQ(Cf) and Q(Cdl) indicate that the capacitance of the SEI film and the electric double layer, respectively. Then, in the low frequency region of the straight line represents the Waberg impedance (W) associated with the Li^+ diffusion coefficient. Table 2 shows that the Rct values of Mg0.02, Na0.02, Na0.02Mg0.01, Na0.02Mg0.02, Na0.02Mg0.03 and Na0.02Mg0.05 are 482.5 Ω, 323.8 Ω, 417.3 Ω, 373.5 Ω, 215.2 Ω, and 638.4 Ω, respectively. The value of the Rct is relatively small. The value of the W is 215.2 Ω when x=0.03 and has the smallest charge transfer resistance value compared to the other samples. The dopant material has a smaller charge transfer resistance value than the pure phase material, which is consistent with the previous electrochemical test results. This indicates that appropriate ion doping can effectively reduce the charge transfer resistance.

$$D_{Li^+}=R^2 \bullet T^2/(2A^2 \bullet n^2 \bullet F^4 \bullet C^2 \bullet \sigma^2) \quad (1)$$

Figure 9 presents the linear fit plots of Z' and $\omega^{-1/2}$ for the prepared samples. The lithium ion diffusion coefficient is calculated by equation (1), where R is the gas constant ($8.314 Jmol^{-1}K^{-1}$), T is the absolute temperature, and A is the surface area of the positive electrode (presumably calculated as 0.785 cm^2), n is the participation of the number of electrons required for a unit reaction, F is the Faraday constant ($96485.33 Cmol^{-1}$), C ($0.0288 molcm^{-3}$) [46] is the application of lithium ions in $LiFePO_4$, and σ is the Wahlberg factor (slope of Figure 9) [47]. It is evident that an appropriate amount of ion doping can effectively improve the lithium ion diffusion coefficient. The Li^+ diffusion coefficients of Mg0.02, Na0.02, Na0.02Mg0.01, Na0.02Mg0.02, Na0.02Mg0.03, and Na0.02Mg0.05 are $1.281\times10^{-14} cm^2s^{-1}$, 2.621×10^{-14} cm^2s^{-1},$1.779\times10^{-14} cm^2s^{-1}$,$3.355\times10^{-14} cm^2s^{-1}$,$4.501\times10^{-14} cm^2s^{-1}$ and $8.799\times10^{-15} cm^2s^{-1}$, respectively. In particular, when x=0.03, the Li^+ diffusion coefficient of the corresponding material Na0.02Mg0.03 is the largest with a value $4.501\times10^{-14} cm^2s^{-1}$, Thus the electrochemical performance of the material is optimal, which is consistent with the previous analysis results. The value of the Li^+ diffusion coefficient in the Na0.02Mg0.05 is $8.799\times10^{-15} cm^2s^{-1}$, which is the smallest. This indicates that Na0.02Mg0.03 displays the best Li^+ diffusion coefficient of the. By adjusting the doping scale of Na^+ and Mg^{2+}, it can improve the coefficient of Li^+ diffusion. The fact is consistent with the reports in some articles previous studies [48-51]. Based on all of the above analysis, the introduction of appropriate Na^+ [52-55] could increase the unit cell parameters, and provide a Li^+ one-dimensional Li^+ diffusion channel in the lattice. At the same time, an appropriate amount of Mg^{2+} doping in the composite system will improve the conductivity and Li^+ diffusion rate of the material. In addition, the cycle and rate performance of the material can be effectively improved by reducing the polarization of the electrode. This method, minimizes cation mixing and and reduces impedance during charge transfer cycles.

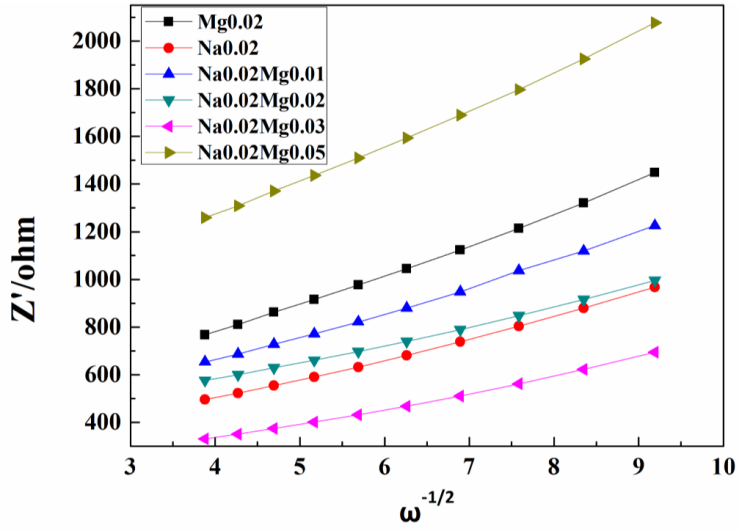

Figure 9. Linear fitting relationship between Z' and $\omega^{-1/2}$ of Mg0.02、Na0.02 and Na0.02Mgx(x=0.01,0.02,0.03,0.05)

Table 3. EIS fitting data of Mg0.02、Na0.02 and Na0.02Mgx (x=0.01,0.02,0.03,0.05)

Samples	$R_s(\Omega)$	$Q(C_f)(F)$	$R_f(\Omega)$	$Q(C_{dl})(F)$	$R_{ct}(\Omega)$	$W/\Omega/s^{1/2}$	$D_{Li^+}(cm^2s^{-1})$
Mg0.02	2.906	2.631×10^{-3}	332.5	1.836×10^{-5}	482.5	1.107×10^{8}	1.281×10^{-14}
Na0.02	2.711	2.011×10^{-3}	225.8	4.19×10^{-5}	323.8	7.273×10^{4}	2.621×10^{-14}
Na0.02Mg0.01	2.866	3.277×10^{-3}	293.6	1.056×10^{-5}	417.3	9.299×10^{6}	1.779×10^{-14}
Na0.02Mg0.02	2.873	4.522×10^{-3}	268.5	7.033×10^{-5}	373.5	9.578×10^{-3}	3.355×10^{-14}
Na0.02Mg0.03	2.715	4.5×10^{-3}	179.7	2.977×10^{-5}	215.2	5087	4.501×10^{-14}
Na0.02Mg0.05	2.91	6.463×10^{-3}	109.4	3.623×10^{-6}	638.4	1.433×10^{-3}	8.799×10^{-15}

4. CONCLUSIONS

In this paper, the samples of Mg0.02、Na0.02 and Na0.02Mgx (x=0.01,0.02,0.03,0.05) composite lithium ion battery cathode material synthesized by a sol-gel method. The results show that a proper amount of Na^+ and Mg^{2+} doping can effectively reduce the impedance of the material and increase the specific capacity and cycle stability of the material. It can be seen from the data that the initial discharge capacity of the corresponding materials of Na0.02, Mg0.02 and Na0.02Mg0.03 in the voltage range of 2.5-4.5V is as high as 139, 136.3 and 147.7 $mAhg^{-1}$, respectively, After charge and discharge cycle at multiple rates that eventually returned to 0.1 C, and the capacity retention rates were 99.4%, 100.44%, and 96.21%, for the Na0.02, Mg0.02, and Na0.02Mg0.03 materials, respectively. In particular, Na0.02Mg0.03 exhibits the highest discharge specific capacity, higher cycle stability and minimum impedance value. Therefore, proper Na^+ and Mg^{2+} doping can obtain better excellent electrochemical performance, mainly because of the improved Li^+ diffusion coefficient and the decrease in the charge transfer resistance value allowing ions to flow more easily and promote the reaction.

References

1. A.K. Padhi, K.S. Nanjundaswamy and J.B. Goodenough, *J. Electrochem. Soc*., 144(1997)1188.
2. P.S. Herle, B. Ellis, N. Coombs and L.F. Nazar, *Nature Mater*., 3(2004)147.
3. F. Zhou, M. Cococcioni, K. Kang and G. Ceder, *Electrochem. Commun*., 6(2004)1144.
4. M. Gaberscek, R. Dominko, M. Bele, M. Remskar, D. Hanzel and J. Jamnik, *Solid State Ionics*, 176(2005)1801.
5. G. Meligrana, C.Gerbaldi, A. Tuel, S. Bodoardo and N. Penazzi, *J. Power Sources*, 160(2006)516.
6. H. Wang, Y. Yang, Y. Liang, L.F.Cui and H. Dai, *Angew. Chem. Int. Ed*., 50(2011)7364.
7. N.S. Norberg and R. Kostecki, *J. Electrochem. Soc*., 159(2012)A1431.
8. J. Moskon, M. Pivko, I. Jerman, E. Tchernychova, N. Zabukovec Logar, M. Zorko, V.S. Selih, R.Dominko and M. Gaberscek, *J. Power Sources*, 303(2016)97.
9. M. Bini, M.C. Mozzati, P. Galinetto, D.Capsoni, S. Ferrari, M. S. Grandi and V. Massarotti, *J. Solid State Chem*., 182(2009)1972.
10. M.R. Roberts, G. Vitins and G. Denuault, *J. Electrochem. Soc*., 157(2010)A381.
11. K. Saravanan, J.J. Vittal, M.V. Reddy, B.V. R. Chowdari and P. Balaya, *J. Solid State Electrochem*., 14(2010)1755.
12. B. Zhang, X. Wang, H. Li and X. Huang, *J. Power Sources*, 196(2011)6992.
13. L. Chen, Y.Y. Qiang, X. Feng and M.W. Li, *J. Power Sources*, 214(2012)344.
14. W. Jun Kwon, I.K. Lee, C. Hyuk Rhee and C.S. Kim, *J. Appl. Phys*., 111(2012)07E139.
15. W. Huang, S. Tao, J. Zhou, C. Si, X. Chen, W. Huang, C. Jin, W. Chu, L. Song and Z. Wu, *J. Phys. Chem. C*., 118(2013)796.
16. D. Bhuvaneswari and N. Kalaiselvi, *Int. J. Electrochem. Sci*., 6(2011)3714.
17. J. Hong, F. Wang, X. Wang and J. Graetz, *J. Power Sources*, 196(2011)3659.
18. C.K. Back, R.Z. Yin and Y.S. Kim, *J. Electrochem. Soc*., 160(2013)A1551.
19. Y.J. Zhong, J.T. Li, Z.G. Wu, X.D. Guo, B.H. Zhong and S.G. Sun, *J. Power Sources*, 234(2013)217.
20. Z.H. Wang, L.X. Yuan, W.X. Zhang and Y.H. Huang, *J. Alloys Compd*., 532(2012)25.
21. H. Shu, X. Wang, Q. Wu, B. Hu, X. Yang, Q. Wei, Q. Liang, Y. Bai, M. Zhou, C. Wu, M. Chen, A. Wang and L. Jiang, *J. Power Sources*, 237(2013)149.
22. Z.H. Wang, L.X. Yuan, M. Wu, D. Sun and Y.H. Huang, *Electrochim. Acta,* 56(2011)8477.
23. H. Shu, X. Wang, W. Wen, Q. Liang, X. Yang, Q. Wei, B. Hu and L. Liu, *Electrochim. Acta,* 89(2013)479.
24. L. Wu, J.J. Lu, G.Wei, P. Wang, H. Ding, J. Zheng, X. Li and S. Zhong, *Electrochim. Acta*, 146(2014)288.
25. L. Gao, Z. Xu and S. Zhang, *J. Alloys Compd*., 739(2018)529.
26. L. Gao, Z. Xu, S. Zhang, J. Xu and K. Tang, *Solid State Ionics*, 305(2017)52.
27. J. Duan, G. Hu and Y.Cao, *Ionics*, 22(2016)609.
28. S. Liu, H. Fang, E. Dai, B. Yang, Y. Yao, W. Ma and Y. Dai, *Electrochim. Acta,* 116(2014)97.
29. K. Kisu, E. Iwama, W. Onishi, W. Onishi, S. Nakashima, W. Naoi and K. Naoi, *J Mater Chem* A, 2(2014)20789.
30. V. Ramar and P. Balaya, *PCCP*, 15(2013)17240.
31. D. Jang, K. Palanisamy, J. Yoon, Y. Kim and W. S. Yoon, *J. Power Sources*, 244(2013)581.
32. H. Yi, C. Hu, H. Fang, B. Yang, Y. Yao and W. Ma, *Int. J. Electrochem. Sci*, 7(2012)663.
33. H. Fang, E. Dai, B. Yang, Y. Yao and W. Ma, *J. Power Sources*, 204(2012)193.
34. H. Yi, C. Hu, H. Fang, B. Yang, Y. Yao, W. Ma and Y. Dai, *Electrochim. Acta*, 56(2011)4052.
35. C. Hu, H. Yi, H. Fang, B. Yang, Y. Yao, W. Ma and Y. Dai, *Electrochem. Commun*., 12(2012)1784.
36. C. Sronsri, P. Noisong and C. Danvirutai, *Spectrochimica Acta Part* A, 153(2016)436.
37. J. Kim, Y.U. Park, D.H. Seo, J. Kim, S.W. Kim and K. Kang, *J. Electrochem. Soc*., 158(2011)A250.

38. W. Xiang, Y. Zhong, Y. Tang, H. Shen, E. Wang and H. Liu, *J. Alloys Compd*., 635(2015)180.
39. H. Yi, C. Hu, X. He and H. Xu, *Ionics*, 21(2015)667.
40. Q.Y. Huang, Z. Wu, J. Su, Y.F. Long, X.Y. Lv and Y.X. Wen, *Ceram. Int*., 42(2016)11348.
41. X.Y. Lv, Q.Y. Huang, Z. Wu, J. Su, Y.F. Long and Y.X. Wen, *J. Solid State Electrochem*., 21(2017)1499.
42. S. Okada, S. Sawa, M. Egashira, J.I. Yamaki, M. Tabuchi and H. Kageyama, *J. Power Sources*, 97(2001)430.
43. J.B. Goodenough, *J. Electrochem. Soc*., 144(1997)1188.
44. J.M. Tarascon and M. Armand, *Nature*, 414(2011)171.
45. C.V. Ramana, A. Ait-Salah, S. Utsunomiya, A. Mauger, F. Gendron and C.M. Julien, *Chem. Mater*. 19 (2007) 5319.
46. H.K. Zhou, J.H. Lu, X.P. Huang, Y.C. Du, F. Liang and Y. C. Yao, SCI *CHINA* TECHNOL SC, 60(2017)1853.
47. L. Dou, E. Han, L. Li, S. Qiao and H. Liu, *Ionics,* 25(2019)2487.
48. J. Zhao, J. He, J. Zhou, Y. Guo, T. Wang, S. Wu, X. Ding, R. Huang and H. Xue, *J PHYS CHEM* C , 115(2011)2888.
49. Y. W. Denis, C. Fietzek and W. Weydanz, *J. Electrochem. Soc*., 154(2007) A253.
50. B. Jin, E. M. Jin, K. H. Parkb and H. B. Gu, *Electrochem. Commun*., 10(2008)1537.
51. J. Li, Q. Qu, L. Zhang, L. Zhang and H. Zheng, *J. Alloys Compd*., 579(2013)377.
52. Z. Chen, T. Xie, L. Li, M. Xu, H. Zhu, W. Wang, *Ionics*, 20(2014):629.
53. W. He, D. Yuan, J.Qian, X. Ai, H. Yang and Y. Cao, *J. Mater. Chem*. A, 1(2013)11397.
54. B. Qiu, J. Wang, Y. Xia, Y. Liu, L. Qin, X. Yao, *J. Power Sources*, 240(2013)530.
55. R. El Khalfaouy, A. Addaou, A. Laajeb and A. Lahsini, *J. Alloys Compd*., 775(2019)836.